Obrabotka metallov (tekhnologiya, oborudovanie, instrumenty) = Metal Working and Material Science. 2026 vol. 28 no. 3 pp. 315–330
ISSN: 1994-6309 (print) / 2541-819X (online)
DOI: 10.17212/1994-6309-2026-28.3-315-330

NSTU NETI

Obrabotka metallov -
Metal Working and Material Science

Journal homepage: http://journals.nstu.ru/obrabotka_metallov

Effect of direct laser deposition process parameters on the microstructure and mechanical properties of new nickel-base superalloys based on ZhS6K

Ilya Astakhov [a, *], *Sofia Korchmarchik* [b], *Margarita Klimova* [c], *Grigoriy Zadykyan* [d], *Rudolf Korsmik* [e], *Nikita Stepanov* [f]

Institute of Laser and Welding Technologies, Saint Petersburg State Marine Technical University, 3 Lotsmanskaya str., Saint Petersburg, 190121, Russian Federation

[a] https://orcid.org/0009-0008-5409-9997, Astakhov@smtu.ru; [b] https://orcid.org/0009-0003-7716-146X, happy23sofia@gmail.com;
[c] https://orcid.org/0000-0002-2188-0209, M.V.klimova@ilwt.smtu.ru; [d] https://orcid.org/0000-0001-7942-2799, gzadykyan@mail.ru;
[e] https://orcid.org/0000-0003-1591-1942, Rudak27@yandex.ru; [f] https://orcid.org/0000-0003-2476-3953, stepanov@corp.smtu.ru

ARTICLE INFO

Article history:
Received: 15 July 2026
Revised: 18 July 2026
Accepted: 14 August 2026
Available online: 15 September 2026

Keywords:
Ni-based superalloys
Additive manufacturing
Technological parameters
Microstructure
Mechanical properties

Funding
This research was funded by the Russian Science Foundation, grant no. 23-19-00622-P.

ABSTRACT

Introduction. Nickel-base superalloys are indispensable materials for hot-section components of gas turbine engines (*GTE*); however, traditional manufacturing of geometrically complex parts is highly time- and resource-consuming. The adoption of additive manufacturing (*AM*), in particular direct laser deposition (*DLD*), enables high-precision fabrication of free-form components. Nevertheless, most nickel-base superalloys with a high volume fraction of the γ' phase (Ni_3Al) are prone to cracking. A promising approach is the development of new alloy compositions specially adapted for *AM*. ***The purpose of this study*** is to investigate Investigation of the influence of *DLD* parameters on cracking behavior, microstructure, and mechanical properties of the previously designed *Ni68* and *Ni75* alloys based on the *ZhS6K* superalloy. **Materials and methods.** Thin-walled specimens were produced by *DLD* with varying laser power, scanning speed, laser spot diameter, and deposition strategy. Cracking susceptibility was evaluated by the specific crack length. Porosity, microstructure, and phase composition were analyzed by optical and scanning electron microscopy. Mechanical properties were assessed by microhardness measurements. **Results and discussion.** A non-linear dependence of the specific crack length on laser power was revealed, with a maximum at 700 W for small spot diameters. The bidirectional deposition strategy was shown to reduce cracking compared with the unidirectional strategy. For the *Ni75* alloy, optimum parameters (power 300 W, speed 3 mm/s, spot diameter 1.0–1.5 mm) under the bidirectional strategy were identified, yielding defect-free specimens with a porosity below 0.2%. It was established that the lower carbon content in Ni75 suppresses carbide precipitation, thus reducing the cracking probability. Increasing the laser power from 300 to 1500 W only weakly affects the transverse grain size, but induces a transition from a near-equiaxed morphology to a columnar one with a pronounced <100> texture; the volume fraction of the strengthening γ' phase remains constant at ~60% for *Ni68* and ~41% for *Ni75*. Microhardness exhibits a weak dependence on the deposition parameters: 390–410 HV for *Ni75* and 430–450 HV for Ni68, indicating the predominant contribution of the γ' phase characteristics. The obtained results demonstrate the applicability of the developed alloys for the additive manufacturing of thin-walled high-temperature components.

For citation: Astakhov I.I., Korchmarchik S.O., Klimova M.V., Zadykyan G., Korsmik R., Stepanov N.D. Effect of direct laser deposition process parameters on the microstructure and mechanical properties of new nickel-base superalloys based on ZhS6K. *Obrabotka metallov (tekhnologiya, oborudovanie, instrumenty) = Metal Working and Material Science*, 2026, vol. 28, no. 3, pp. 315–330. DOI: 10.17212/1994-6309-2026-28.3-315-330. (In Russian).

Introduction

Nickel-base superalloys (*Ni*-superalloys) are key structural materials in modern gas turbine engines (*GTE*). Owing to their combination of physical and mechanical properties at elevated temperatures, this class of materials is used to manufacture engine components operating at the highest temperatures [1].

*** Corresponding author**
Astakhov Ilya Ivanovich, Engineer
Institute of Laser and Welding Technologies,
Saint Petersburg State Marine Technical University,
3 Lotsmanskaya str.,
190121, Saint Petersburg, Russian Federation
Тел.: +7 930 087-99-93, **e-mail:** Astakhov@smtu.ru

The structure of nickel-base superalloys that provides the best high-temperature performance is an *FCC* matrix with a high volume fraction (over 50%) of strengthening $L1_2$-type intermetallic γ′-phase (Ni_3Al) particles. For example, the domestic *ZhS6K* alloy belongs to the class of cast nickel-base superalloys and is widely used for manufacturing *GTE* rotor and nozzle blades owing to its optimal balance of heat resistance and castability. However, the fabrication of geometrically complex parts involves a lengthy and resource-intensive process cycle that includes multi-stage mechanical and heat treatment [2].

One promising solution is the use of layer-by-layer 3*D*-printing technologies, in particular direct laser deposition (*DLD*). This method is among the most advanced in additive manufacturing (*AM*), since it enables the fabrication of components of any geometric shape and size while providing high productivity and manufacturing precision, and it can also be used for the local repair of failed components [3–5]. The main obstacle to the widespread adoption of additive manufacturing for *Ni*-superalloy components is the poor weldability of most nickel alloys with a high content of the strengthening γ′ phase. Because of the similarity between the thermal processes involved in *AM* and welding, most superalloys are prone to defects such as hot and cold cracks, lack of fusion, and porosity.

To suppress cracking, the first approach is usually optimization of the deposition parameters; however, this does not always yield substantial results for conventional alloys with a high γ′-phase fraction [6, 7]. Another approach involves developing new alloy compositions specially adapted for *AM* [8]. To prevent hot cracking, new alloys must combine a narrow solidification range with a minimal liquid-phase fraction at the final stages of solidification [9]. Furthermore, it is fundamentally important to retain a high volume fraction of the γ′ phase. It is likewise important to lower the solvus temperature of secondary phases, including carbides, borides, and topologically close-packed (*TCP*) phases.

Thus, in a previous study [10], a high-throughput *CALPHAD*-based approach was used to design, on the basis of the *ZhS6K* alloy, two promising alloy compositions adapted for additive manufacturing with the above requirements taken into account. However, that study [10] focused on producing bulk specimens, so the obtained results have limited applicability to thin-walled components. For practical tasks such as manufacturing thin-walled structural elements (e.g., *GTE* blades with cooling channels [11]) or the local repair of *Ni*-superalloy components, an in-depth understanding of the materials' cracking susceptibility at minimal wall thickness is required. Thin-walled structures are known to be highly sensitive to fluctuations in thermal conditions during additive manufacturing, which can lead to substantial inhomogeneity of the microstructure and properties [12].

The purpose of this study was to investigate the effect of *DLD* parameters on the cracking behavior, structure, and mechanical properties of thin-walled specimens of new alloys developed on the basis of *ZhS6K*. To achieve this goal, ***the following tasks*** were addressed:

– to determine the optimal *DLD* parameters (laser power, scanning speed, laser spot diameter, and build strategy) that provide a defect-free structure in thin-walled specimens;

– to investigate the effect of laser power on the morphology, size, and crystallographic texture of the grains, as well as on the phase composition, including the morphology and volume fraction of the strengthening γ′ phase and secondary-phase particles;

– to evaluate the mechanical properties of the alloys as a function of the *DLD* process parameters and to compare the obtained values with the characteristics of bulk specimens.

Methodology, materials, and equipment

In a previous study [10], a high-throughput *CALPHAD*-based approach was used to propose two promising compositions for new nickel alloys. The alloys were designated *Ni68* and *Ni75*, where the numbers denote the calculated nickel content of 68 and 75 wt.%, respectively.

The selected alloy compositions were produced as metal powders by gas atomization at *Polema JSC* (*Tula*, Russia). Incoming inspection of the new-alloy powders revealed a predominantly spherical particle morphology with a small proportion of irregularly shaped particles and the presence of surface satellites (Fig. 1). The powder particle-size distribution ranged from 40 to 150 μm. The average particle size was 83 μm and 95 μm for *Ni68* and *Ni75*, respectively.

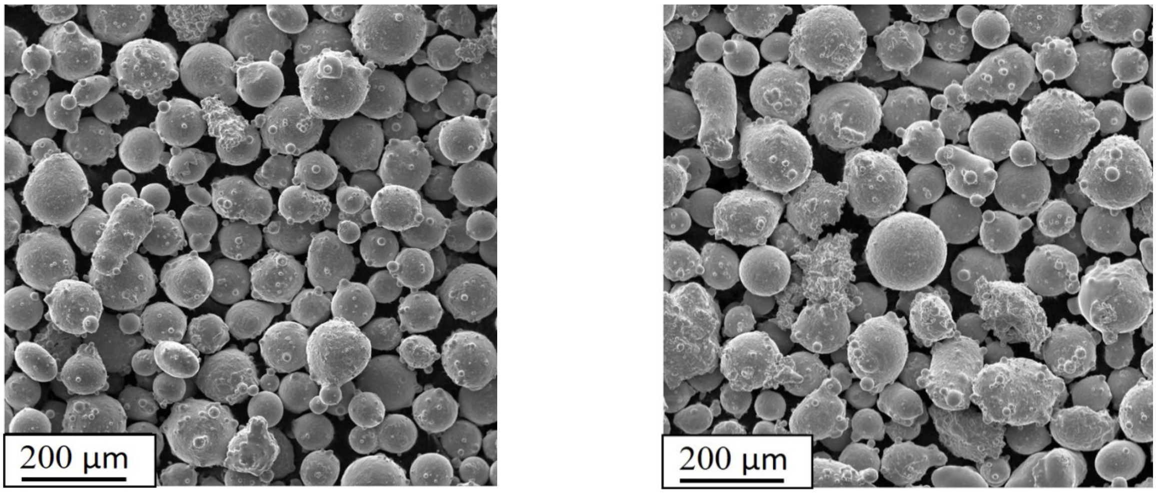

a *b*

Fig. 1. SEM images of powder particles of (*a*) *Ni68* and (*b*) *Ni75* alloys

The chemical composition of the alloys was analyzed by energy-dispersive X-ray spectroscopy (*EDS*). The actual composition of the powders is given in Table 1. The nitrogen and oxygen contents were determined by inert-gas fusion using a *Meteck-600* analyzer; the gas concentrations did not exceed 0.004% and 0.009%, respectively. The carbon mass fraction, measured with a *Meteck-200* analyzer, was 0.100% and 0.085% for the *Ni68* and *Ni75* alloys, respectively.

Table 1

Actual elemental composition of powders, wt. %

Alloy	*Ni*	*Al*	*Cr*	*Ti*	*Mo*	*W*	*Mn*	*Fe*	*S*	N_2	O_2	*C*
Ni68	68.89	6.84	8.50	1.22	3.71	5.52	0.21	1.24	<0.001	0.013	0.009	0.100
Ni75	73.3	4.09	8.65	2.0	2.83	4.93	0.15	0.71	<0.001	0.004	0.006	0.085

Direct laser deposition of the thin-walled specimens was carried out using an *ILIST-M* processing unit (*SMTU*, Russia) equipped with an *IPG YLR-1500-U* ytterbium fiber laser with a 100 µm core diameter (Fig. 2). The laser beam was focused onto the substrate surface using an *IPG FLW D30* processing head (*IPG Photonics*, USA), forming a highly concentrated energy source. Metal powder was delivered into the melt pool through a powder feeder with a 5 L hopper capacity. During deposition, the powder melted in the laser-beam interaction zone and solidified as a single bead; layer-by-layer overlapping of the beads along a preset trajectory produced the bulk specimen. The motion of the processing tool was performed by an *M-10iD/12* welding robot (*Fanuc*, *Oshino*, Japan). Cooling of the optical system during deposition was provided by an *SMC HRSH090-A-40* chiller.

To determine the *DLD* process parameters that provide defect-free thin-walled specimens with dimensions of 50×20×2 mm^3, a series of experiments was carried out with varying processing conditions and scanning strategies. Two wall-deposition strategies were investigated – unidirectional and bidirectional. Under the unidirectional strategy, the laser moved in one direction while its return to the starting position was performed in idle mode, which increased the pauses between passes. Under the bidirectional strategy, the laser moved alternately in both directions, which minimized the pauses between passes and produced a reheating and/or partial remelting effect on the previously deposited metal during the return pass.

The following process parameters were varied in the experiment: laser power ***P*** (300, 700, 1,100, and 1,500 W), laser travel speed ***V*** (3, 10, 17, and 25 mm/s), laser spot diameter ***D*** (1.0, 1.5, 2.0, and 2.5 mm), and powder mass flow rate ***G*** (from 1.8 to 20 g/min). Combining these factors resulted in 24 different deposition regimes being implemented for each of the developed alloys (Table 2).

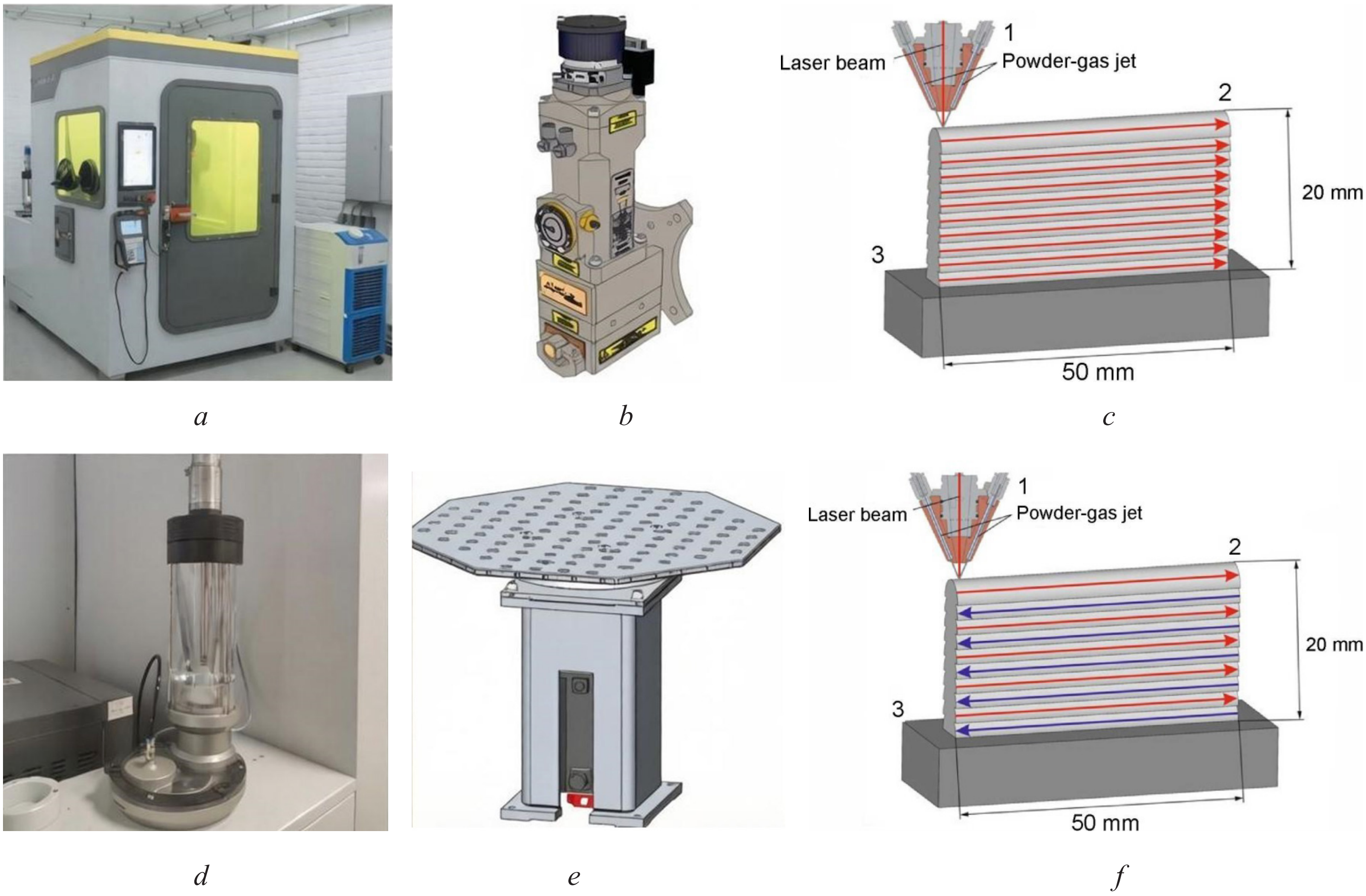

Fig. 2. ILIST-M process unit (*a*); *IPG* processing head (*b*); powder feeder (*d*); single-axis positioner (*e*); unidirectional (*c*) and bidirectional (*f*) deposition strategies

Table 2

Deposition modes for thin walls of Ni68 and Ni75 alloys

Mode No.		Laser power (***P***, W)	Scanning speed (***V***, mm/s)	Laser spot diameter (***D***, mm)	Powder feed rate (***G***, g/min)
Unidirectional	Bidirectional				
1	13	300	3	1.0	2.2
2	14	700	10	1.0	4.5
3	15	300	3	1.5	1.9
4	16	700	10	1.5	5.0
5	17	1,100	17	1.5	10.5
6	18	1500	25	1.5	19.5
7	19	700	10	2.0	7.0
8	20	1,100	17	2.0	12.0
9	21	1,500	25	2.0	20.0
10	22	700	10	2.5	6.5
11	23	1,100	17	2.5	11.0
12	24	1,500	25	2.5	20.0

Initial quality control of the deposited walls was performed by analyzing digital images of the specimen surface to detect surface cracks. Quantitative assessment of cracking susceptibility was carried out using *Digimizer v.6* software (*MedCalc Software*, Belgium). For each image, all visible cracks were identified, their length measured, and their total number counted. Based on the obtained data, the specific crack length parameter was calculated as the ratio of the total length of all detected cracks to the total area of the analyzed specimen surface ($\boldsymbol{P} = Lsum/S$, where $Lsum$ is the total crack length and S is the cross-sectional area).

Surface preparation of the specimens for subsequent structural studies was carried out using a colloidal *SiO_2* suspension on a *Model 200 Dimpling Grinder* (*Thermo Fisher Scientific Inc.*, USA). Macrostructure and porosity were examined using a *Leica DMi8* optical microscope (*Leica Microsystems*, *Wetzlar*, Germany). The porosity value was determined from five optical surface images as the ratio of the total pore area to the total area. Microstructural analysis was performed using a *SEM* equipped with an electron backscatter diffraction (*EBSD*) detector with *AZtecCrystal 2.2* software (*Oxford Instruments NanoAnalysis*, *Abingdon*, UK), as well as an energy-dispersive spectroscopy (*EDS*) detector (*Ultim Max 65*).

To establish the relationship between the mechanical properties and the deposition regimes, microhardness tests were carried out. *Vickers* hardness was measured on a *Future-Tech FM-310* instrument (*Future-Tech Corp.*, *Kawasaki*, Japan) with a 300 g applied load; at least 20 measurements were performed for each state.

Results and discussion

Initial visual and dimensional inspection of the obtained specimens revealed a substantial effect of the deposition parameters and strategy on cracking (Fig. 3). Under the unidirectional strategy, a large number of surface cracks formed in the alloys, oriented predominantly along the deposition direction. Switching to the bidirectional deposition strategy produced a dramatic improvement in surface quality: a significant reduction in the number of cracks was observed in the alloys. This pronounced positive effect of the bidirectional strategy may be attributed to a more uniform temperature field in the build zone and a reduction in thermal-stress gradients owing to reheating and partial remelting of the previously deposited layer during the return pass of the laser [13].

To quantitatively assess cracking as a function of the process parameters, the specific length of visible cracks was measured. Fig. 4 shows the dependence of the specific crack length on laser power for the different scanning strategies. A non-linear dependence was revealed for both alloys, regardless of the

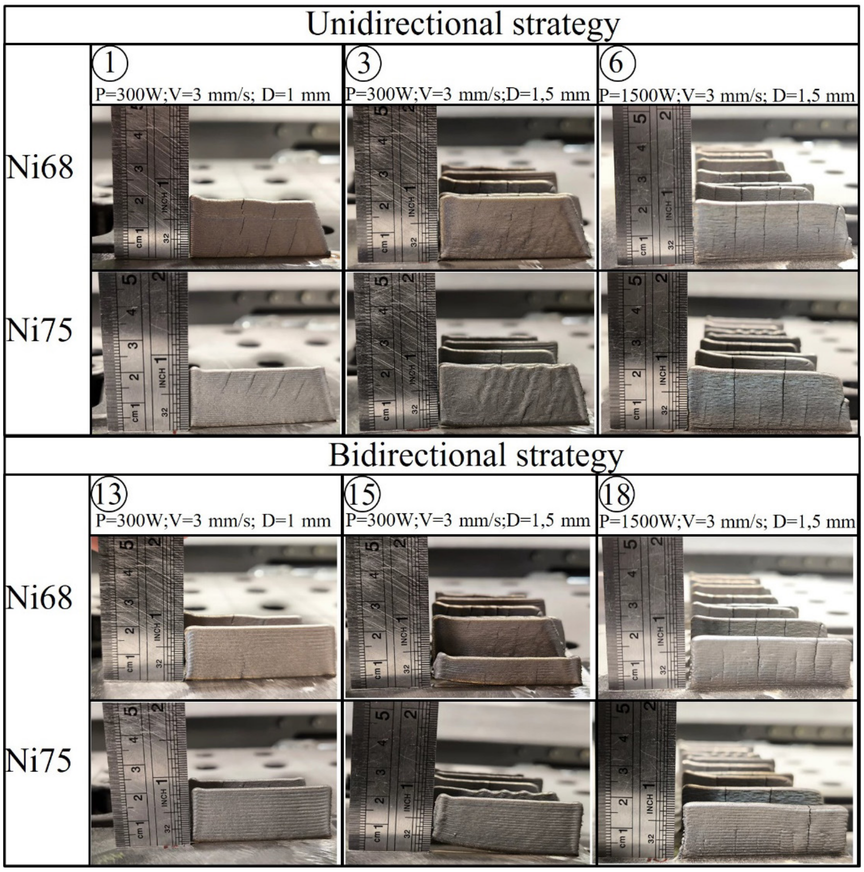

Fig. 3. Appearance of thin walls deposited under different processing conditions

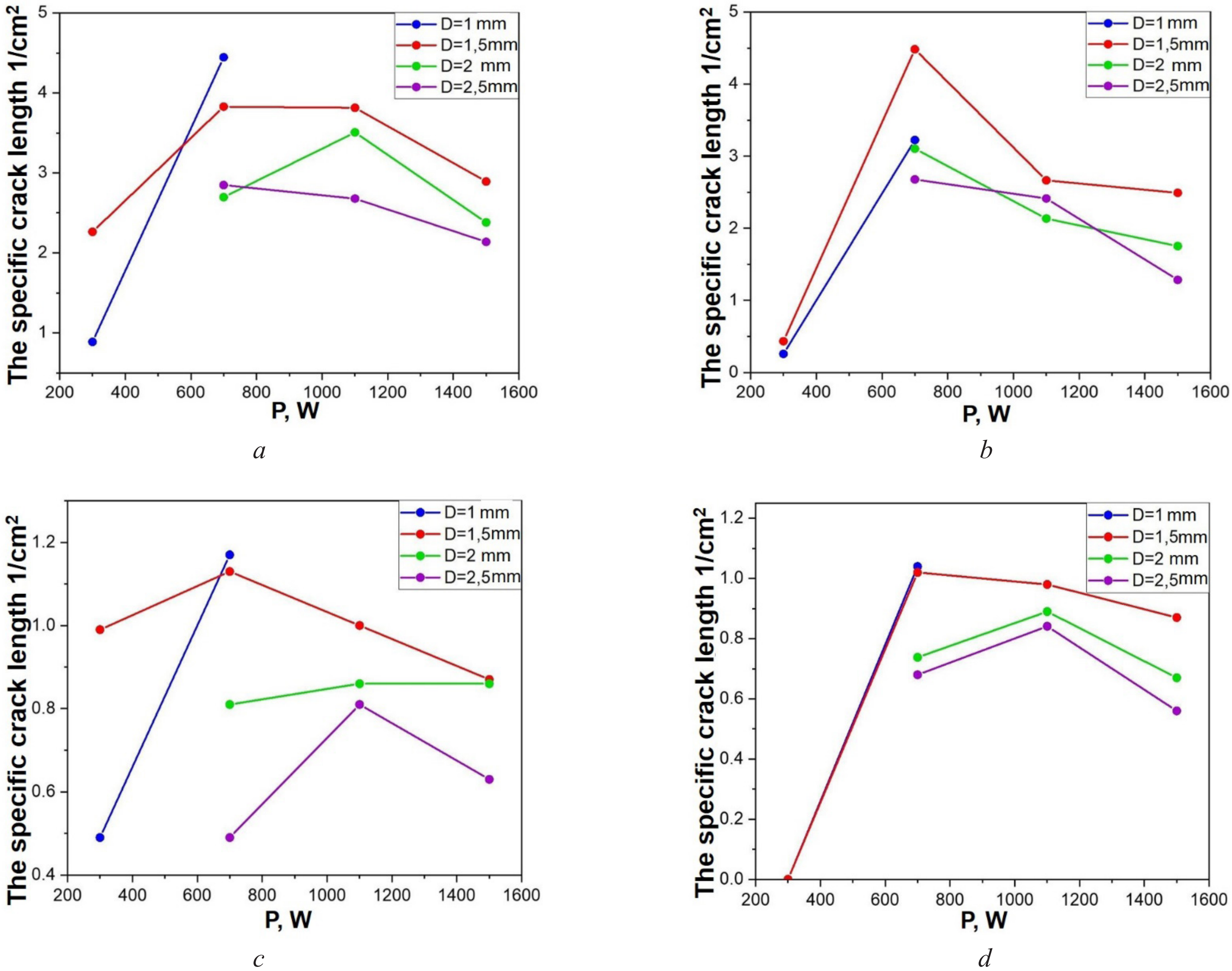

Fig. 4. Dependence of specific crack length on laser power for (*a*, *b*) *Ni68* and (*c*, *d*) *Ni75* alloys under (*a*, *c*) unidirectional and (*b*, *d*) bidirectional deposition strategies

chosen strategy and spot size. The lowest specific crack length values were observed under the low-energy mode with a power of 300 W. As the power increases, the specific length rises, reaches a peak value, and then decreases. It was shown that for a laser spot diameter of 1.0 and 1.5 mm, the peak value for both alloys occurs at a power of 700 W. Increasing the spot diameter to 2.0 and 2.5 mm shifts this peak toward higher power values – 1,100 W.

It is also worth noting the lower cracking susceptibility of the *Ni75* alloy: the maximum specific crack length does not exceed 1.2 cm^{-1}, whereas for the *Ni68* alloy this value reaches 4.5 cm^{-1} (Fig. 4). It was further established that two modes (modes No. 13 and No. 15) under the bidirectional strategy with a power of 300 W and spot sizes of 1.0 and 1.5 mm yield walls of the *Ni75* alloy free of surface cracks.

Analysis of the alloy macrostructure by optical microscopy showed that, depending on the selected mode, various defects may form in the material: hot cracks, lack of fusion, unmelted powder particles, and porosity. For further study, alloy specimens produced using the bidirectional strategy were selected: the low-energy mode No. 15 (power 300 W), which provides a state with a minimal crack fraction (in the case of Ni68) and a fully defect-free state (in the case of *Ni75*). In addition, the high-energy mode No. 18 (power 1,500 W) was also selected for both alloys for comparative analysis. It is shown (Fig. 5) that deposition using mode No. 18 is characterized, for both alloys, by extensive cracking with numerous vertical cracks. In turn, the use of mode No. 15 in the *Ni68* alloy reduced the number and size of cracks, which were predominantly localized at the specimen/substrate interface, whereas for the *Ni75* alloy it enabled a defect-free structure to be obtained with a high relative density and a pore volume fraction not exceeding 0.2%.

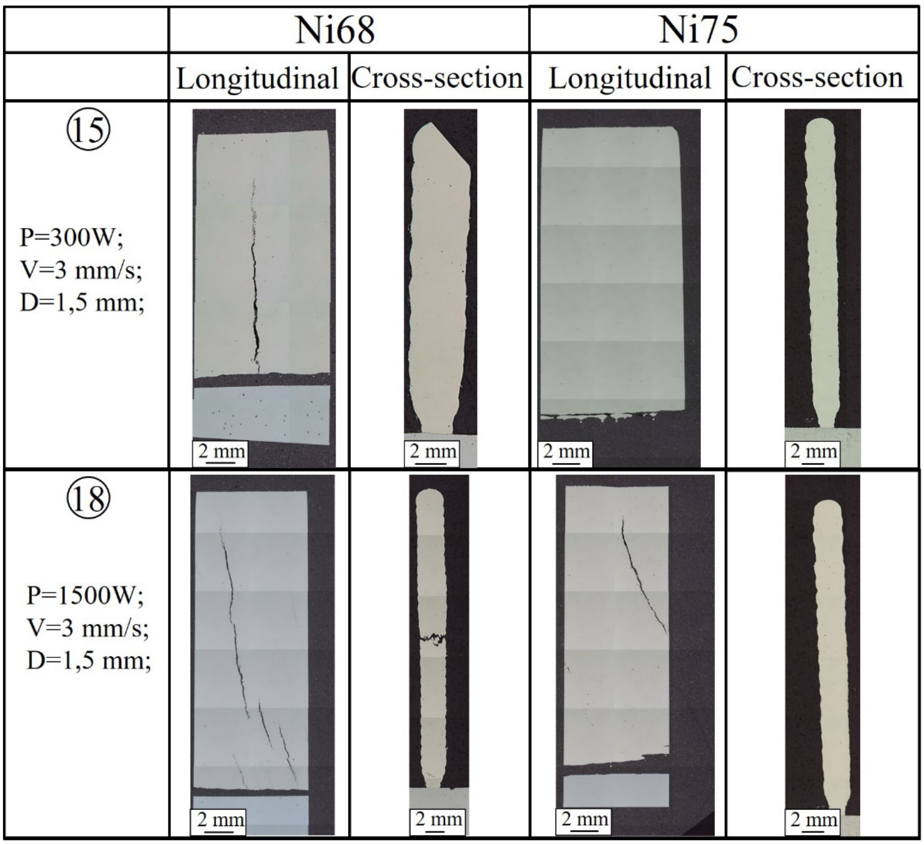

Fig. 5. Macrostructure of *Ni68* and *Ni75* alloys

The microstructure of the deposited walls formed under different *DLD* parameters was studied by *SEM*. Fig. 6 shows the results of *EBSD* analysis of the grain structure of the *Ni68* (Fig. 6,*a*, *b*) and *Ni75* (Fig. 6,*c*, *d*) alloys, deposited at powers of 300 W and 1,500 W. The alloy structure consists of an *FCC* matrix with elongated grains oriented along the deposition direction and a texture close to <100>. In the alloys deposited at 300 W, in addition to columnar grains, the presence of near-equiaxed grains was noted, with the fraction of such grains in the *Ni68* alloy being higher. Increasing the process power to 1,500 W results in the formation of an exclusively columnar structure. The transformation of the microstructure from equiaxed to columnar is explained by an increase in the temperature gradient (***G***) at the solidification front with increasing process power. As shown in studies on nickel alloys in *AM* [12], a change in the ratio of the temperature gradient to the solidification rate (***G***/***R***) is a key factor that shifts the solidification conditions in favor of the directional growth of pre-existing grains and suppresses the nucleation of new equiaxed grains. Nevertheless, it should be noted that increasing the power has practically no effect on the transverse grain size, which in the *Ni68* and *Ni75* alloys was 120 μm and 100 μm at 300 W and increases only slightly to 140 μm and 130 μm at 1,500 W, respectively.

SEM examination of the microstructure in the longitudinal section demonstrates the formation of a dendritic structure oriented in two directions, which follows the changing trajectory of the laser-beam motion in both alloys. In the *Ni68* alloy, the enrichment of the interdendritic regions in *Ti*, *Mo*, and *W* is caused by intracrystalline segregation at the final stages of solidification, when the melt enriched in these alloying elements solidifies last [10, 11]. *EDS* mapping revealed the presence of two types of particles differing in chemical composition, with a total volume fraction of 1.4%. Coarse particles about 1 μm in size, enriched in *Mo* and *W*, are probably Me_6C-type carbides and are located predominantly in the interdendritic regions. *Ti*-enriched carbides, probably of the *MeC* type, are more uniformly distributed within the structure and are considerably smaller (below 0.5 μm). Cracks oriented along grain and dendrite boundaries were additionally detected, probably of segregation origin, since their development was characteristic of regions with an elevated fraction of secondary phases.

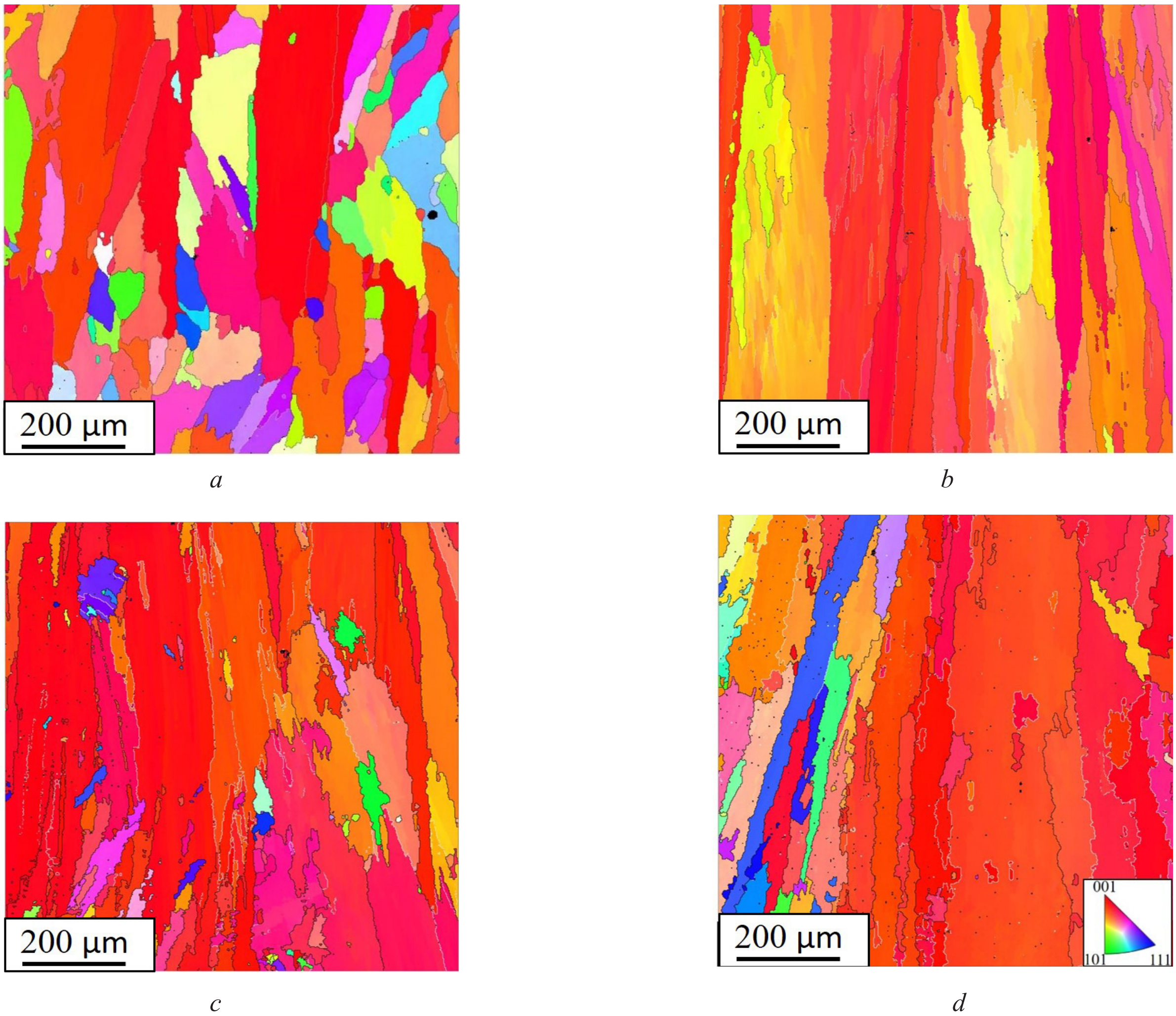

Fig. 6. EBSD images of (*a*, *b*) *Ni68* and (*c*, *d*) *Ni75* alloys in transverse cross-section, deposited at laser powers of (*a*, *c*) 300 W and (*b*, *d*) 1,500 W under a bidirectional strategy

In the *Ni75* alloy, a similar structure with dual dendrite orientation is observed; however, the phase composition merits separate attention (Fig. 7). In the alloy microstructure, secondary-phase precipitates were practically absent: only isolated *Ti*-rich *MeC*-type carbides were detected in the interdendritic regions. This is directly related to the substantially lower carbon content in the initial powder of the *Ni75* alloy, since below a critical carbon concentration the precipitation of the carbide phase becomes both thermodynamically and kinetically hindered [1]. It should be noted that the phase composition of the alloys did not depend on the process power.

High-magnification electron images obtained with a backscattered-electron detector were used to evaluate the morphology, volume fraction, and average size of the strengthening γ' phase. In the *Ni68* alloy (Fig. 8,*a*), the γ'-phase particles exhibit the cuboidal morphology typical of *Ni*-superalloys, with an average size of 60 nm and a volume fraction of 60%, which is characteristic of the prototype *ZhS6K* alloy. In the *Ni75* alloy (Fig. 8,*b*), the particle volume fraction was substantially lower, at 41%, and the intermetallic particles had a spherical morphology with a bimodal size distribution: larger particles (50 nm) in the interdendritic space and smaller particles (<30 nm) at the dendrite cores. A similar bimodal distribution has previously been reported in other nickel alloys produced by *AM* [14–16]. It is also worth noting that increasing the process power did not substantially affect the size or volume fraction of the strengthening phase.

Fig. 9 shows the results of microhardness measurements of the thin alloy walls as a function of laser power. Analysis of the mechanical characteristics of the alloys revealed no significant changes in properties with varying power. It was established that the *Ni75* alloy shows average microhardness values in the range of 390–410 HV, which is lower than that for *Ni68* (430–450 HV). The lower microhardness of *Ni75* is

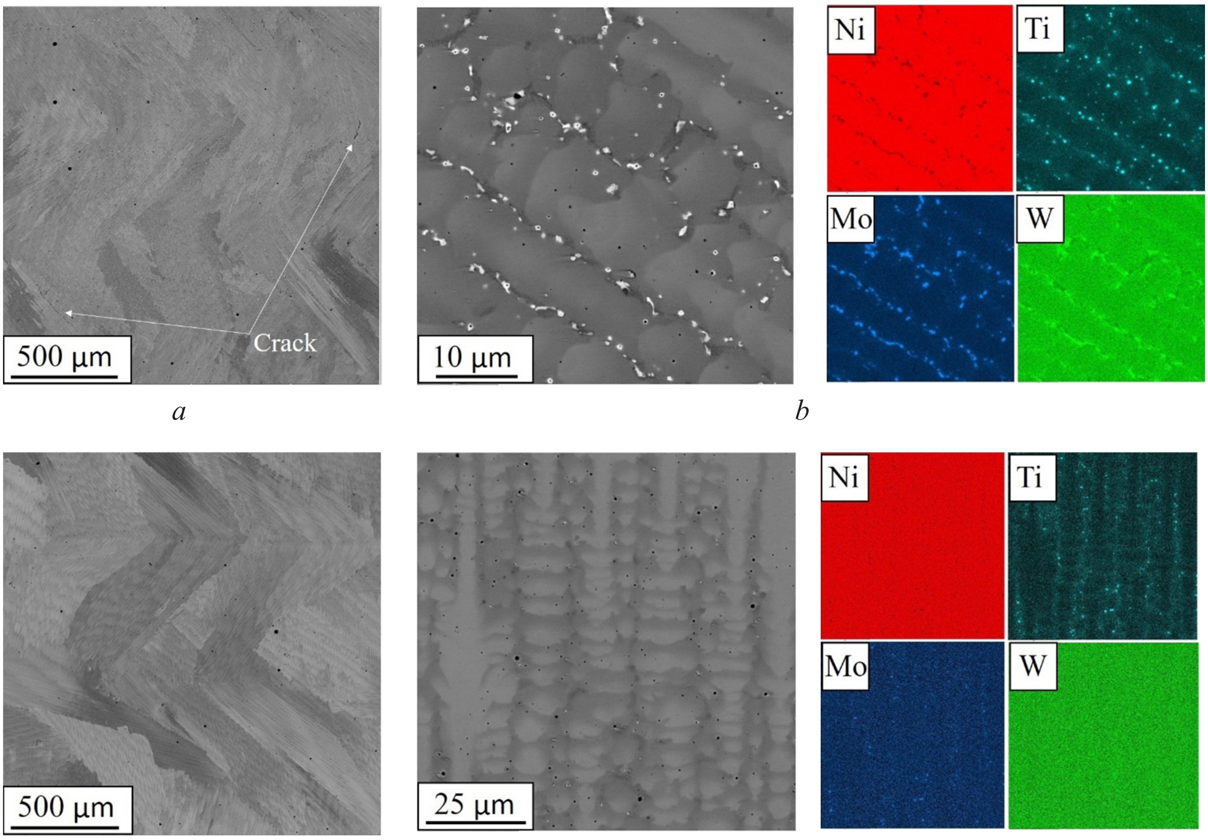

a *b*

c *d*

Fig. 7. Microstructure (*a*, *c*) and *EDS* mapping (*b*, *d*) of (*a*, *b*) *Ni68* and (*c*, *d*) *Ni75* alloys in longitudinal section, deposited at a laser power of 300 W under a bidirectional strategy

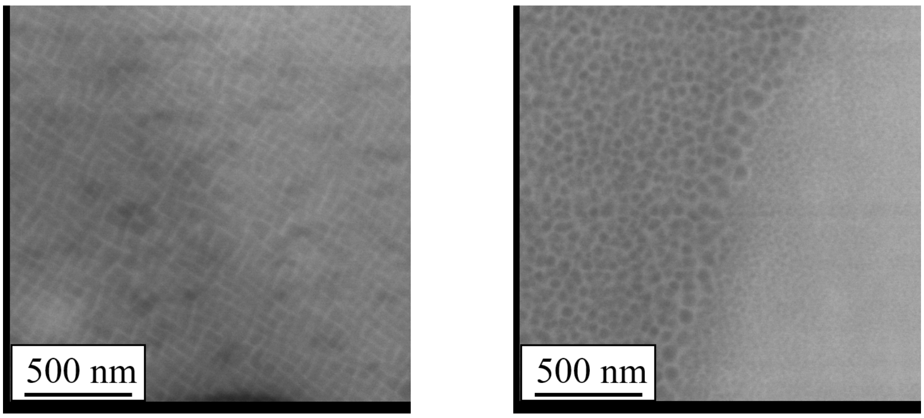

a *b*

Fig. 8. SEM images of γ′-phase morphology in (*a*) *Ni68* and (*b*) *Ni75* alloys, deposited at a laser power of 300 W under a bidirectional strategy

related to the smaller volume fraction of the strengthening γ′ phase compared with *Ni68*. Since the strength properties of nickel alloys are governed to a greater extent by the parameters (volume fraction and size) of the strengthening phase rather than by differences in the grain structure [17], the close microhardness values obtained when varying the laser power are entirely expected.

Comparison with the microhardness results for bulk billets from [10] showed that the thin walls exhibit microhardness values comparable to (for *Ni68*) or exceeding (for *Ni75*) those of the bulk material, and are therefore expected to show high strength characteristics. Moreover, the mechanical properties of the additively manufactured new alloys (Table 3) can exceed those of the conventional cast and heat-treated *ZhS6K* alloy [18, 19].

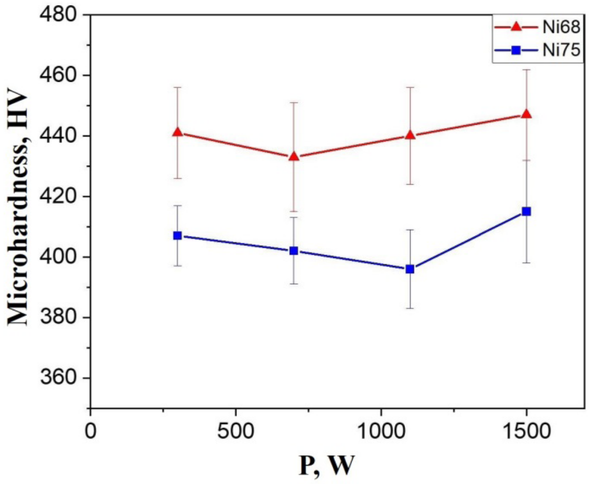

Fig. 9. Dependence of microhardness on laser power for the alloys

Table 3

Mechanical properties of alloys at 25 °C

Alloy	Condition	Microhardness (HV)	Yield strength (MPa)	Ultimate strength (MPa)
Ni68	Thin walls samples	447 ± 15	–	–
Ni75		415 ± 17	–	–
Ni68	Bulk samples [10]	440 ± 6	900 ± 4	1,271 ± 37
Ni75		375 ± 4	789 ± 25	1,222 ± 40
ZhS6K	As-cast condition [18]	–	895	1,000
ZhS6K	Heat-treated [19]	–	800	878

The results of the present study demonstrate the advantage of the bidirectional deposition strategy over the unidirectional one for manufacturing thin-walled parts. Compared with *ZhS6K*, the new alloys exhibit better manufacturability under additive manufacturing conditions; however, a fully defect-free structure can be obtained only for the *Ni75* alloy. As a measure for further reducing the cracking susceptibility of the *Ni68* alloy, it would be advisable to use substrate preheating, which reduces the thermal gradients during deposition [20, 21], as well as subsequent heat treatment aimed at relieving internal stresses and modifying the phase composition [22].

Conclusions

New alloys developed on the basis of *ZhS6K* were produced as thin-walled specimens by direct laser deposition. Based on the results of the study, the following conclusions were drawn:

1. Switching from the unidirectional to the bidirectional deposition strategy reduced the cracking susceptibility of the thin-walled specimens. The *Ni75* alloy demonstrated better manufacturability under *AM* conditions compared with the *Ni68* alloy. Using modes with a power of 300 W made it possible to obtain, in the *Ni75* alloy, a defect-free structure with a porosity below 0.2%.

2. The microstructure of the alloys is an *FCC* matrix with grains elongated along the deposition direction and a crystallographic orientation close to <100>. Increasing the process power from 300 W to 1,500 W results in the formation of a fully columnar structure and has no effect on the phase composition of the alloys.

3. The *Ni68* alloy is characterized by a high volume fraction of cuboidal γ′ phase (60%) and the presence of *MeC*- and Me_6C-type carbides, predominantly in the interdendritic regions. In the *Ni75* alloy, the fraction of spherical γ′ phase is 41%, and the lower carbon content limits secondary-phase precipitation, thereby reducing the risk of liquation cracking along the grain boundaries.

4. The *Ni68* alloy exhibits higher microhardness values (430–450 HV) than the *Ni75* alloy (390–410 HV), which correlates with the difference in γ′-phase volume fractions. The strength characteristics of the thin walls are comparable to those of additively manufactured bulk specimens of these alloys and exceed those of the cast, heat-treated *ZhS6K* alloy.

References

1. Reed R.C. *The superalloys: fundamentals and applications*. Cambridge, Cambridge University Press, 2008. 388 p. ISBN 978-1-139-45863-4.

2. Kablov E.N., ed. *Litye lopatki gazoturbinnykh dvigatelei: splavy, tekhnologii, pokrytiya* [Cast blades of gas turbine engines: alloys, technologies, coatings]. 2nd ed. Moscow, Nauka Publ., 2006. 632 p. ISBN 5-02-034270-X.

3. Tukov S., Korsmik R., Zadykyan G., Mukin D., Mendagaliev R., Roschin N. Development of a laser cladding technology for repairing first-stage high-pressure turbine blades in gas turbine engines. *Metals*, 2025, vol. 15 (9), p. 957. DOI: 10.3390/met15090957.

4. Zadykyan G.G., Korsmik R.S., Gushchina M.O., Zhukov A.S., Promakhov V.V. Research and development of technology for obtaining small-scale GTE parts from ceramic composite materials by 3D printing. *Journal of Physics: Conference Series*, 2018, vol. 1109 (1), p. 012057. DOI: 10.1088/1742-6596/1109/1/012057.

5. Zemlyakov E., Babkin K., Korsmik R., Sklyar M., Kuznetsov M. Perspektivy ispol'zovaniya tekhnologii lazernoi naplavki dlya vosstanovleniya lopatok kompressorov gazoturbinnykh dvigatelei [Prospects for the use of laser cladding technology for the repair of compressor blades of gas turbine engines]. *Fotonika = Photonics Russia*, 2016, no. 4, pp. 10–25. DOI: 10.22184/1993-7296.2016.58.4.10.22.

6. Raevskikh A.N., Chabina E.B., Filonova E.V. Effect of initial powder characteristics on microrelief features in the ZhS6K grade alloy after selective laser fusion. *Inorganic Materials: Applied Research*, 2022, vol. 13 (6), pp. 1592–1604. DOI: 10.1134/S207511332206020X.

7. Dmitrieva A., Semenyuk A., Klimova M., Udin I., Mukin D., Vildanov A., Zherebtsov S., Klimova-Korsmik O., Stepanov N. Cracking behavior of the ZhS6K superalloy during direct laser deposition with induction heating. *Metals*, 2024, vol. 14 (6), p. 610. DOI: 10.3390/met14060610.

8. Zhu L., Wei B., Wang K., Zhou C., Ji H. Optimizing selective laser melting of a high-alloyed Ni-based superalloy: achieving crack-free fabrication with enhanced microstructure and mechanical properties. *Acta Metallurgica Sinica (English Letters)*, 2025, vol. 38 (10), pp. 1719–1734. DOI: 10.1007/s40195-025-01900-7.

9. Markanday J.F.S. Applications of alloy design to cracking resistance of additively manufactured Ni-based alloys. *Materials Science and Technology*, 2022, vol. 38 (16), pp. 1300–1314. DOI: 10.1080/02670836.2022.2068759.

10. Klimova M., Astakhov I., Klimenko D., Zadykyan G., Klimova-Korsmik O., Korsmik R., Stepanov N. Tailoring ZhS6K-based Ni superalloys for laser-based directed energy deposition. *Journal of Alloys and Compounds*, 2026, vol. 1058, p. 186956. DOI: 10.1016/j.jallcom.2026.186956.

11. Momeni S., Gargarella P., Rodrigues A.R., Jasinevicius R.G. Fabrication of thin-walled Inconel 718 microchannels by LP-DED: influence of deposition strategy on geometric fidelity, surface texture, and post-processing feasibility via hybrid manufacturing. *The International Journal of Advanced Manufacturing Technology*, 2026, vol. 144 (9–10), pp. 7009–7032. DOI: 10.1007/s00170-026-18255-7.

12. Zhang X., Wang S., Liang Y., Guo Y., Guo Z., Yi F., Lin J. Laser directed energy deposition of thin-walled GH4099 superalloy with gradient microstructure and mechanical properties. *Materials Science and Engineering: A*, 2025, vol. 933, p. 148283. DOI: 10.1016/j.msea.2025.148283.

13. Zhang X., Chen H., Xu L., Xu J., Ren X., Chen X. Cracking mechanism and susceptibility of laser melting deposited Inconel 738 superalloy. *Materials & Design*, 2019, vol. 183, p. 108105. DOI: 10.1016/j.matdes.2019.108105.

14. Barjesteh M.M., Abbasi S.M., Madar K.Z., Shirvani K. The effect of heat treatment on characteristics of the gamma prime phase and hardness of the nickel-based superalloy Rene® 80. *Materials Chemistry and Physics*, 2019, vol. 227, pp. 46–55. DOI: 10.1016/j.matchemphys.2019.01.038.

15. Klimova M., Astakhov I., Yurchenko N., Zadyukyan G., Klimenko D., Klimova-Korsmik O., Korsmik R., Turichin G., Zherebtsov S., Stepanov N. Microstructure and mechanical properties of gradient Rene 41/Rene 80 superalloy, fabricated by laser-based directed energy deposition. *Journal of Alloys and Compounds*, 2025, vol. 1048, p. 185270. DOI: 10.1016/j.jallcom.2025.185270.

16. Guzman I., Granda E., Mendez R., Lopez G., Acevedo J., Gonzalez D. Particle size of gamma prime as a result of vacuum heat treatment of INCONEL 738 super alloy. *Journal of Materials Engineering and Performance*, 2013, vol. 22 (4), pp. 1143–1148. DOI: 10.1007/s11665-012-0385-y.

17. Goodfellow A.J. Strengthening mechanisms in polycrystalline nickel-based superalloys. *Materials Science and Technology*, 2018, vol. 34 (15), pp. 1793–1808. DOI: 10.1080/02670836.2018.1461594.

18. Kuznetsov V.P., Lesnikov V.P., Popov N.A. *Struktura i svoistva monokristallicheskikh zharoprochnykh nikelevykh splavov* [Structure and properties of single-crystal heat-resistant nickel alloys]. Ekaterinburg, Ural University Press, 2016. 160 p. ISBN 978-5-7996-1829-2.

19. Khimushin F.F. *Zharoprochnye stali i splavy* [Heat-resistant steels and alloys]. 2nd ed., rev. Moscow, Metallurgiya Publ., 1969. 752 p.

20. Jin Z., Kong X., Ma L. Investigating the impact of substrate preheating on the thermal flow and microstructure of laser cladding of nickel-based superalloy. *Materials*, 2024, vol. 17 (2), p. 399. DOI: 10.3390/ma17020399.

21. Gulov M.A., Gertsel I.S., Malikov A.G. Additional substrate heating in direct laser deposition of Inconel 738. *Physical Mesomechanics*, 2026, vol. 29 (1), pp. 115–126. DOI: 10.1134/S1029959925600910.

22. Huang M., Zhou Z., Cui C., Zhang R., Shi Z., Wang X., Zhou Y., Sun X. Formation and evolution behavior of M6C carbide in a Ni-W-Cr superalloy. *Materials Characterization*, 2023, vol. 204, p. 113211. DOI: 10.1016/j.matchar.2023.113211.

Conflicts of Interest

The authors declare no conflict of interest.